The Onset of Convection in the Madden–Julian Oscillation

SUSAN R. KEMBALL-COOK AND BRYAN C. WEARE

Department of Land, Air, and Water Resources, University of California, Davis, Davis, California

(Manuscript received 23 August 1999, in final form 3 February 2000)

ABSTRACT

An observational study of the onset of convection in the Madden–Julian oscillation (MJO) was performed. Composites of radiosonde data from the Comprehensive Aerological Reference Data Set were constructed for an ensemble of tropical stations located in the Indian Ocean, Maritime Continent, and western Pacific Ocean.

The composites suggest that for the off-equatorial stations used in this study, the MJO period may be set by the buildup and discharge of the low-level moist static energy. This result supports the discharge–recharge hypothesis of Bladé and Hartmann. MJO events appear to begin when the off-equatorial atmosphere has been destabilized through a combination of low-level moist static energy buildup and concurrent drying of the middle troposphere by subsidence in the wake of the previous cycle of MJO convection. The low-level moist static energy buildup is controlled by a corresponding increase in low-level moisture. The increase in low-level moisture is not caused by the 1000-mb convergence. For the stations examined here, the convergence lags the moist static energy buildup and is instead in phase with the convection.

1. Introduction

The Madden–Julian oscillation (MJO) was first identified by Madden and Julian (1971, 1972) as an eastward-propagating anomaly in the tropical winds and surface pressure having a period of 30–60 days. The anomalous circulation has a simple baroclinic structure and is characterized by a region of upward motion associated with deep convection and adjacent regions of downwelling and suppressed convection. A review of observations of the MJO is given in Madden and Julian (1994), and a summary of theoretical work may be found in Waliser et al. (1999).

Theories of the MJO must explain the large-scale nature and eastward propagation of the anomalies and also their 30–60-day periodicity. Much of the theoretical and modeling work on the MJO has focused on the eastward propagation of the convective anomaly and on its interaction with the large-scale circulation (Hendon and Salby 1994; Salby et al. 1994; Wang and Li 1994; etc.). While the structure and energetics (Hendon and Salby 1994) of the MJO have been well documented, relatively little attention has been paid to the causes of the initial appearance and organization of convection in the Indian Ocean. There has been no definitive explanation for the 30–60-day period of the MJO.

Corresponding author address: Susan R. Kemball-Cook, Department of Meteorology, University of Hawaii at Manoa, Honolulu, HI 96822.
E-mail: suekc@soest.hawaii.edu

The purpose of this study is to examine the composited thermodynamic and kinetic structure of MJO convection in order to investigate its initiation. The method used is to employ radiosonde data for a set of tropical stations combined with large-scale satellite and reanalysis datasets to form a composite picture of the onset of MJO convection at a station. In section 2, an overview of previous studies concerning the initiation of MJO convection is given. In section 3, the datasets and method used in this study are discussed. Section 4 is a description of the radiosonde composites of the onset of convection, and, in section 5, a summary and discussion of the results are provided.

2. Brief review of studies of MJO onset

There are three types of explanations for the onset of convection in the MJO. In the first type, convection in the Indian Ocean is triggered by an extratropical event, whereas in the second and third types, convection results from an internal tropical interaction between convection and the large-scale circulation.

a. Extratropical triggers

In an observational case study of an MJO event, Hsu et al. (1990) found evidence suggesting that Rossby wave trains propagating into the Tropics from the midlatitudes may play a role in organizing convection in the MJO. Hsu et al. saw an extratropical Rossby wave arrive in the Indian Ocean, followed by rapid in situ development of a region of upward vertical velocity at

500 mb. They inferred that this upward motion induced convection and started the next cycle of the MJO. A composite study of the 200-mb streamfunction performed as part of the present work (Kemball-Cook 1999) showed little evidence of systematic initiation of convection by the incursion of extratropical waves into the Indian Ocean. Bladé and Hartmann (1993) caution, however, that these Rossby waves may be stochastically forced and may not appear in a composite study.

b. Internal tropical triggering by circumnavigating signal

In many wave–CISK model studies of the MJO, the explanation for the triggering of MJO convection is that the convection anomalies re-emerge over Africa or the Indian Ocean as a result of the arrival of the circulation anomaly radiating from the previous cycle of the MJO (Hendon 1988; Knutson et al. 1986; Bladé and Hartmann 1993, etc.). The periodicity of the oscillation is set by the time needed for the upper-level circulation anomaly to travel around the world and return to the Indian Ocean. This is particularly true of modeling studies in which the domain consists of an equatorial channel (e.g., Wang and Li 1994). Though studies of composite MJO events suggest some evidence for circumnavigation of the globe by an upper-level disturbance (Rui and Wang 1990; Knutson and Weickmann 1987), case studies of individual MJO events (Hsu et al. 1990) do not bear this out. Furthermore, it is unclear physically how an upper-level zonal wind or divergence anomaly would trigger MJO convection (Bladé and Hartmann 1993). There is also some question as to the aptness of the use of the upper-level velocity potential used in Knutson and Weickmann (1987) to show the circumnavigation of the MJO signal (Bladé and Hartmann 1993). Hendon and Salby (1994) reasoned that because the MJO convection signal becomes uncorrelated with itself after one cycle, the Kelvin response emanating from the previous cycle is not essential to the initiation of the next.

c. Internal tropical triggering by discharge–recharge

An alternative explanation for the triggering of MJO convection in the Indian Ocean is that the discharge and recharge of local convective instability contributes to the initiation of convection. The one-dimensional modeling study of Hu and Randall (1994) showed that interactions among radiation, convection, and surface fluxes can set up an oscillating diabatic heat source with a period similar to that of the MJO. The timescale of the oscillation is determined by the radiation–convection–surface interaction and is primarily controlled by the long timescale of radiative cooling. The convection can then destabilize eastward-propagating modes that make up the MJO circulation anomalies as in Gill (1980). Thus, it is not necessary to invoke large-scale wave motions to explain the observed oscillations in convection.

The discharge–recharge theory of Bladé and Hartmann (1993) suggests that both internal mode and extratropical triggering mechanisms may be at work. For certain parameter spaces in their modeling study, they saw circumnavigation of an upper-level wind signal, which then initiated the next MJO event. However, when they prohibited the signal from traveling around the world by adjusting the sea surface temperature in the Western Hemisphere, the MJO still existed with a period similar to that of the prior case. They concluded that local oscillations of the static stability may contribute to the timing of MJO convective episodes. The MJO period is determined by the recharge time for moist static energy in the region of the Indian Ocean where MJO convection usually begins together with the time required for the convective event. Once the atmosphere becomes unstable to convection, any trigger could start the next MJO cycle, and the most likely candidate, as determined by their model, is extratropical waves (Bladé and Hartmann 1993). Another modeling study that suggests that the discharge and recharge of moist static energy may play a role in the MJO is that of Wang and Schlesinger (1999). By effectively requiring convection in a GCM to be triggered by the buildup of low-level moist static energy, they constrained the model MJO to occur with a frequency closer to that which is observed.

An observational study of the Australian monsoon by Hendon and Liebmann (1990) lends support to the discharge–recharge hypothesis. They found that the passage of MJO convective events over Australia dried and stabilized the lower troposphere, making further convection impossible until low-level moisture had built back up again. Their plot of moist static energy taken at Darwin confirms Bladé and Hartmann's conjecture that the static stability oscillates based on the phase of the MJO (Bladé and Hartmann 1993). Hendon and Liebmann's study, however, focused on the end of the MJO convective event, not its onset, and no thermodynamic trigger was found for initiation of the MJO. Bladé and Hartmann (1993) suggest that this is because Darwin is located in the middle of the convective region where the oscillation is induced by wave propagation, not by local thermodynamics, and that an examination of station data for the MJO onset region in the Indian Ocean might yield information about such a trigger.

Studies of the life cycle of the MJO have been performed using satellite and reanalysis data (e.g., Rui and Wang 1990; Knutson and Weickmann 1987; Hendon and Salby 1994). Because reanalyses are generated by models based on observations, which are sparse in the Indian Ocean, the vertical structure of the atmosphere away from radiosonde stations there is highly dependent on model boundary layer and convection physics (Kalnay et al. 1996). It is useful, therefore, to supplement the large-scale picture of the MJO gained from the reanalyses with radiosonde observations in order to gain

a more complete picture of the vertical structure of the atmosphere. This type of study has been done for the Australian monsoon (Mapes and Houze 1992; Hendon and Liebmann 1990) and for the limited time period of the Tropical Oceans and Global Atmosphere Coupled Ocean–Atmosphere Response Experiment (TOGA COARE) Intensive Observing Period (IOP, Lin and Johnson 1996). The aim of the present study, then, is to employ multiyear radiosonde observations to investigate the local physical processes associated with the onset of MJO events at stations in the Indian and western Pacific Oceans. The primary method of analysis is the derivation of composites of variables relative to the passage of MJO events over a radiosonde station.

3. Data and method

a. Compositing procedure

The compositing strategy for this study was to select an ensemble of MJO events that occurred over a 3-yr period and use them to form an average event. Individual MJO events were identified by their convective signal, as convection is the process of interest here. To be included in the composite, MJO events were required to have a convective anomaly that appeared in the Indian Ocean and then propagated eastward into the western Pacific Ocean. Once a set of suitable events was identified, each event was examined in turn to see if it passed over any of the radiosonde stations for which sounding data were available. For each radiosonde station, a subset of the MJO events that passed overhead was identified. Composites of thermodynamic variables (temperature, specific humidity, etc.) for that station were constructed based on the subset of events that passed over the station.

Once composites for all variables for all radiosonde stations were completed, it was found that the station composites for each variable were similar enough that a station grand mean composite could be formed for each variable. This was done for all variables by averaging together all the individual station composites of that variable.

b. Cloud data and filtering

Maps of outgoing longwave radiation (OLR) for the period 1975–90 and brightness temperature (T_b) for 1988–90 were used to identify regions of enhanced and suppressed convection associated with the MJO. The National Oceanic and Atmospheric Administration outgoing longwave radiation (NOAA OLR) dataset (Liebmann and Smith 1996) contains interpolated daily maps of OLR data collected by polar orbiting satellites, and the International Satellite Cloud Climatology Project (ISCCP) C1 dataset (Rossow and Gardner 1993) contains 3-hourly maps of T_b data from both geostationary and polar orbiting satellites. From these 3-hourly maps, daily averages were calculated.

To isolate the MJO signal in convection, the OLR and T_b datasets were filtered. Since the period of the MJO convection has been reported to be anywhere from 20–80 days (Madden and Julian 1994), a broadband filter encompassing the 10–100-day band was used in order to retain all relevant variability in the OLR and T_b. The filtering procedure used was that of Rui and Wang (1990) and produces a map of pentad mean anomalies of OLR and T_b for each day.

Once maps of OLR and T_b pentad mean anomalies (PMAs) were created, individual MJO events were identified using the procedure of Rui and Wang (1990). The filtered OLR was averaged over the region −7.5°S–7.5°N in latitude. These averages were used to create Hovmoeller diagrams of OLR. To be classified as an MJO event, the Hovmoeller diagram OLR anomalies had to satisfy the following criteria (Rui and Wang 1990).

1) Lifespan of the OLR anomaly is greater than four pentads.
2) During its entire lifespan, the zonal dimension of the anomaly must exceed 30° in longitude.
3) Central OLR anomaly must be less than -15 W m^{-2}.
4) At its strongest stage of evolution, the zonal dimension must be larger than 50° in longitude, and its OLR anomaly must be less than -25 W m^{-2}.

MJO events identified in this manner were included in the composite if they fell between 15 September and 30 April. These dates bracket the equinoxes and were chosen because the convective signal is weaker and of different character in the boreal summer (Hartmann and Gross 1988; Wang and Rui 1990).

c. Radiosonde data

Radiosonde soundings from the Comprehensive Aerological Reference Data Set (CARDS) (Eskridge et al. 1995) were used to create composite time series of relevant variables for each radiosonde station. Radiosonde stations were chosen to encompass the entire MJO convective region (Fig. 1). Though a total of 45 stations were examined during this study, only the 17 stations in Fig. 1 had enough data for the years 1988–90 to form statistically stable composites. Data coverage is therefore sparse, and the lack of stations on the equator is a serious problem.

Radiosonde soundings are often plagued with missing or bad data (Eskridge et al. 1995), and although the CARDS dataset is quality controlled, several additional steps were taken to ensure that the soundings used in this study were physically reasonable (Kemball-Cook 1999). After these initial data checks, missing data points at the mandatory levels were filled by linear interpolation in time, producing a daily average value at each mandatory level. In order to take advantage of significant levels reported in the soundings, the soundings were interpolated in the vertical using a cubic Her-

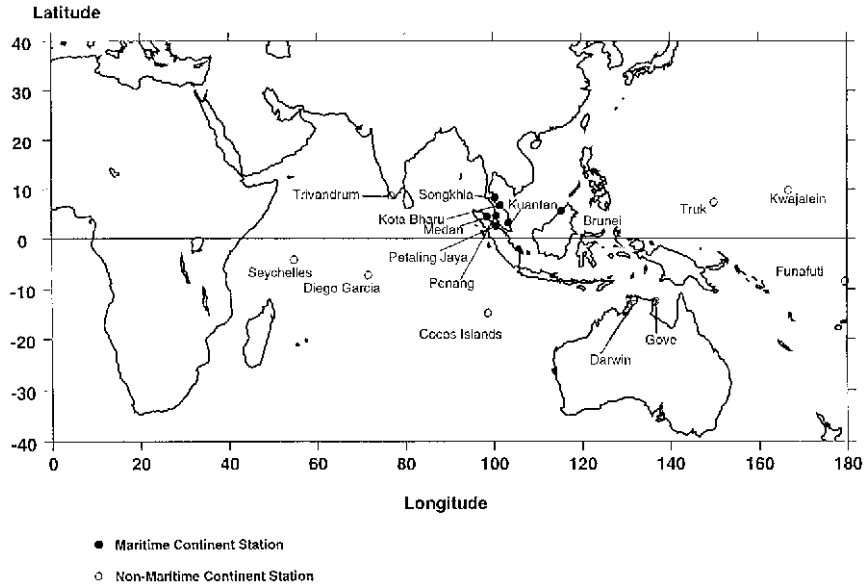

FIG. 1. CARDS data stations.

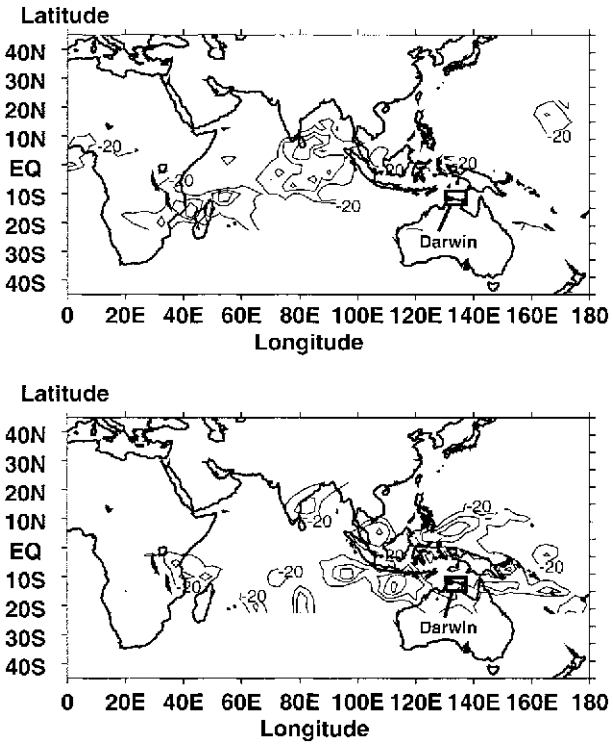

FIG. 2. OLR Anomaly for day −10 and day 0 relative to MJO onset at Darwin. Contours are negative OLR anomaly. Contour interval is 20 W m^{-2} and contours range from −90 to −5 W m^{-2}. Negative OLR anomaly indicates the presence of enhanced convection.

mite polynomial interpolation (Press et al. 1986). This produces for each sounding a smooth profile with 25 pressure levels, retaining as many of the significant layers near the surface as possible. Sounding data varied in temporal resolution from station to station from thrice daily to daily or less. For each station, a daily average vertically interpolated sounding was produced for use in this study.

d. Compositing of radiosonde observations

An OLR PMA animation was used to track the negative OLR anomaly for each MJO event to determine whether that event passed over each of the individual radiosonde stations. If the answer was yes, then that event was included in that station's composite. It is difficult to define the precise day on which the onset of deep convection occurs, because the convective phase of the MJO is characterized by shallow convection building to deep convection as time passes (Lin and Johnson 1996). For convenience, the start date for a particular event at a station was chosen to be the day on which the PMA OLR became less than 0 W m^{-2} near the time of the arrival of the negative OLR anomaly associated with the large-scale MJO convective envelope. Figure 2 shows the negative OLR anomaly for an event that organized over the Indian Ocean on day −10 (relative to onset at Darwin) and later arrived in the vicinity of Darwin on day 0.

Because the OLR and T_b data are not highly filtered, there is convection present that is not associated with the MJO. This higher wavenumber variance is retained in order to capture smaller-scale features that might be important in triggering the onset of convection. Westward-moving convection is not filtered out and it is

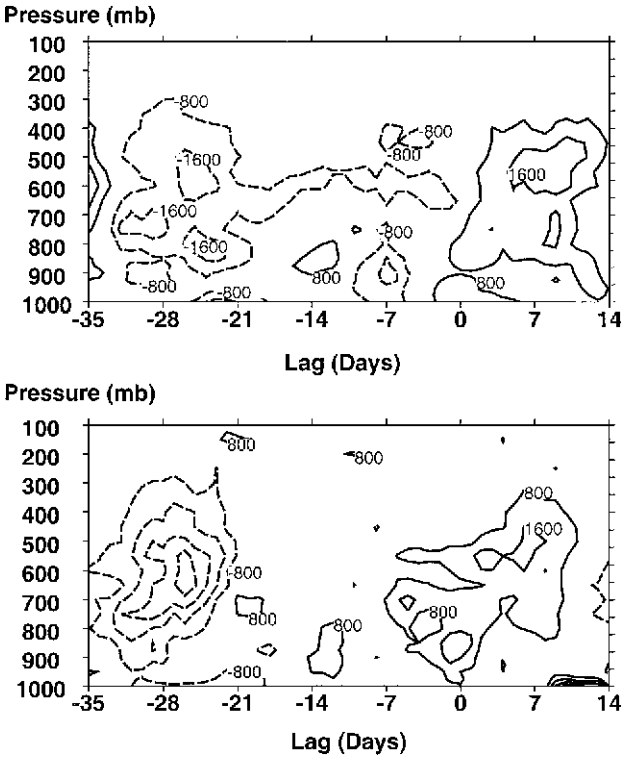

FIG. 3. Comparison of Diego Garcia moist static energy anomalies for the years 1988–90 (top) and 1975–90 (bottom). Solid contours indicate positive moist static energy anomaly and dashed contours indicate negative moist static energy anomaly. Contour interval is 600 J kg^{-1}.

therefore occasionally difficult to say which clusters of clouds are associated with the MJO and which are not.

The composites are formed from 3 yr of data, 1988–90. As only eight MJO events fitting the selection criteria occurred during this time period, time series for all CARDS variables extending from 1975 to 1990 for Diego Garcia, Darwin, and Trivandrum were examined to see if the composites for the shorter period matched those from the long period reasonably well. Figure 3 shows the moist static energy composite for Diego Garcia for the time periods 1975–90 and 1988–90. Moist static energy is defined $h = C_pT + Lq + gz$, where C_p is the specific heat of air, T is air temperature, L is the latent heat of condensation, q is the specific humidity, g is the gravitational constant, and z is the geopotential height. Though the composite for 1988–90 is noisier than the composite for 1975–90, the basic features are similar enough to make the use of the shorter time period reasonable. Results similar to those in Fig. 3 were obtained for the other CARDS stations and for the other variables used in this study. The two exceptions were the Australian stations Darwin and Gove Airport, which were excluded from the 3-yr composites because their OLR anomalies were found to have a shorter average period during the years 1988–90 (~45 days) than during the years 1975–90 (~55 days).

e. NCEP–NCAR reanalysis data

Data from the NCEP–NCAR reanalysis (Kalnay et al. 1996) for the period 1975–90 were used to examine large-scale circulations and thermal structures associated with the MJO. The reanalysis fields are on a 2.5° × 2.5° grid and are available as daily averages. Reanalysis variables used in this study are zonal and meridional wind, vertical pressure velocity (dp/dt)(ω), temperature, specific humidity, and geopotential height.

4. Results

a. Radiosonde station composites

The basic features of the Madden–Julian oscillation as captured by the CARDS station composites are described below. All quantities are filtered pentad mean anomalies unless otherwise indicated.

1) OLR AND T_b COMPOSITES

Figure 4 shows composite OLR anomaly time series for the period 1975–90 for Diego Garcia, Trivandrum, Darwin, and Funafuti. These stations were selected because together they encompass much of the convective region of the MJO. They show remarkable similarity in their OLR composites, particularly in the magnitude of the negative anomaly during the convective event.

The OLR anomaly is positive during the suppressed phase of the oscillation (Rui and Wang 1990), indicating an anomalously small amount of deep convection. As the onset of convection approaches, the positive anomaly builds, reaching a maximum on day −3. Then, the OLR anomaly drops off quickly, passing through 0 K on day 0. The OLR anomaly reaches a minimum on day +4. The convective event lasts about 15 days, after which the OLR anomaly is positive once more. The OLR anomaly has a period of about 55 days for these four stations.

Figure 4 also allows a look at the intrastation variability of the OLR anomaly. This figure includes both land (Trivandrum, Darwin) and atoll (Diego Garcia, Funafuti) stations, which are widely separated in space. In spite of their geographic differences, these stations have 15-yr OLR anomaly composites that are very similar.

Station composites of T_b for the period 1988–90 were compared to station composites of OLR for the period 1975–90 for all CARDS stations. The OLR and T_b composites were similar enough that we can conclude that a 3-yr T_b time series is sufficient to form a reasonable composite of MJO convective activity for all stations except Gove Airport and Darwin, which were excluded from the compositing procedure.

The remaining CARDS stations were divided into two groups: those that are located in the Maritime Continent (MC) and those that are not (non-MC). It has been noted in other studies (Rui and Wang 1990; Salby and Hendon

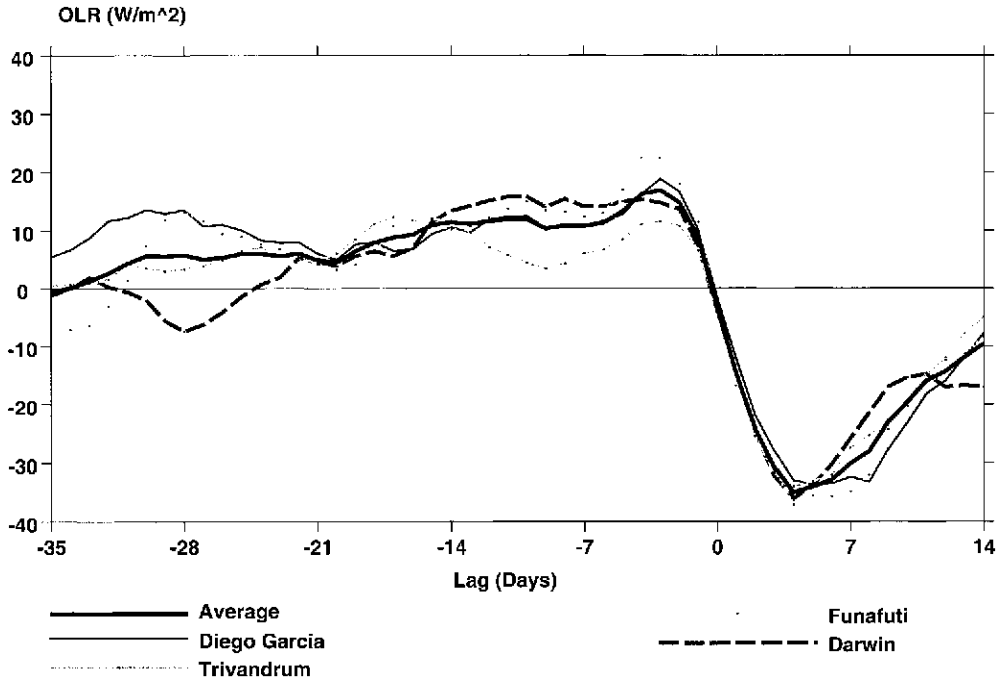

FIG. 4. Station composite OLR anomalies. Horizontal axis is lag in days. Thick solid line is the average of the OLR anomalies of the four stations shown.

1994; etc.) that both deep convection and its suppression are more pronounced in the non-MC regions. Zhang and Hendon (1997) and Nitta et al. (1992) suggest that the strong diurnal cycle of convection over land in the Maritime Continent discharges convective instability so efficiently that strong MJO convection never forms there. OLR was composited separately for MC and non-MC stations. The most noticeable difference between the MC and non-MC OLR curves is that the amplitude of the non-MC curve is larger; qualitatively, they are very similar.

Comparison of the composites of MC and non-MC stations for thermodynamic variables as well as OLR showed that basic features for non-MC and MC stations were similar; however, the MC station anomalies were generally smaller in magnitude and noisier. Because the signal strength of the non-MC stations is greater, only non-MC composites will be shown from here on.

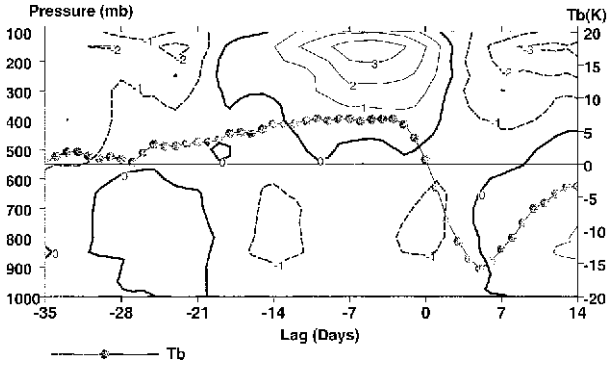

FIG. 5. Non–Maritime Continent station composite zonal wind and T_b anomalies. Thin solid contours indicate positive (westerly) zonal wind anomaly and dashed contours indicate negative (easterly) zonal wind anomaly. Thick solid line is the 0 contour. Contour interval is 1 m s^{-1}.

2) ZONAL WIND COMPOSITE

Figure 5 shows the composite zonal wind anomaly for the non-MC stations. The period from day −35 to day −20 is characterized by anomalous upper-level easterlies and weak low-level wind anomalies, with light lower-level anomalous westerlies centered around 800 mb. During the phase of the MJO when convection is most strongly suppressed (day −20 to day 0), the upper-level anomalous winds are westerly, and the lower-level anomalous winds are weak and easterly. After the convection is well underway, the upper-level anomalous westerlies are replaced by easterly anomalies, which reach their maximum at day +8. After the onset of convection, the low-level anomalous easterlies are replaced by westerlies. Figure 5 shows that low-level westerly wind anomalies arrive about four days after the onset of deep convection, with peak anomalous wind speed occurring about two weeks after the onset of convection. This matches the timing of the westerly wind bursts observed following the three MJO events, which occurred during the TOGA COARE IOP (Lin and Johnson 1996).

This simple first baroclinic mode wind structure is characteristic of the MJO (Madden and Julian 1972).

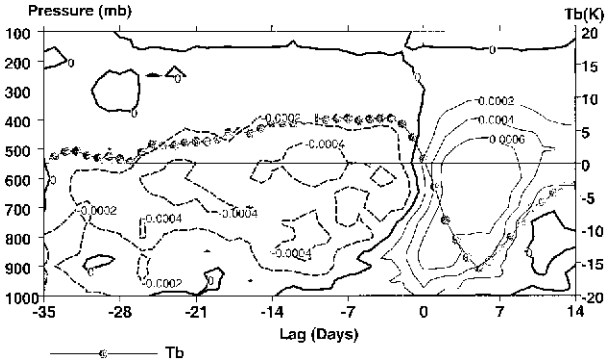

FIG. 6. Non–Maritime Continent station composite specific humidity and T_b anomalies. Thin solid contours indicate positive specific humidity anomaly and dashed contours indicate negative specific humidity anomaly. Thick solid line is the 0 contour. Contour interval is 0.0002 kg kg^{-1}.

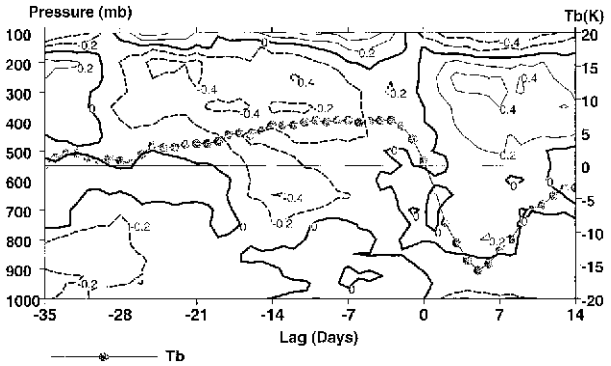

FIG. 7. Non–Maritime Continent station composite temperature and T_b anomalies. Thin solid contours indicate positive temperature anomaly and dashed contours indicate negative temperature anomaly. Thick solid line is the 0 contour. Contour interval is 0.2 K.

Because the upper-level anomalous easterlies do not arrive until after deep convection begins, there is little evidence here for Kelvin wave initiation of convection, which would require the arrival of upper-level easterly anomalies before the onset of the convection. This echoes the results seen in the NCEP–NCAR 200-mb zonal wind spatial composite (not shown) in which the upper-level easterly anomalies appear over the Indian Ocean at the same time as the MJO convection and appear to be caused by upper-level divergence due to deep convection.

3) SPECIFIC HUMIDITY COMPOSITE

Figure 6 shows the specific humidity (q) anomaly composite for the non-MC stations. The suppressed phase of the MJO cycle is characterized by a dry anomaly that extends from 400 mb down to about 950 mb and lasts nearly until the onset of convection in the next MJO cycle. The anomalously dry region reaches its maximum intensity in the middle troposphere and helps create strong static stability that inhibits further deep convection. Starting about two weeks before the onset of MJO convection, the dry anomaly in the lower troposphere begins to erode, possibly due to moistening by shallow convection. As deep convection begins, a strong positive q anomaly centered at 600 mb grows in the midtroposphere. This anomaly, which reaches a maximum at day +5, is likely created by evaporation of detrained condensate introduced into the free troposphere by deep convection (Yanai et al. 1973; Lin and Johnson 1996). The upward movement of anomalous moisture with time as convection can be clearly seen in Fig. 6. Meanwhile, at the lowest levels of the atmosphere, a dry anomaly appears starting at about day +3. Presumably, this drying is caused by the introduction of low θ_e air from the middle troposphere into the boundary layer through the action of convective downdrafts (Betts 1976). By day +10, the intensity of the convection has lessened and the positive q anomaly begins to fade and, by day +20, is replaced by a deep negative anomaly (not shown).

In Fig. 6, there is evidence for preconditioning of the atmosphere for convection during the two weeks before onset. From day −14 to day 0 there is a gradual increase in the positive water vapor anomaly with altitude. A possible mechanism for this moistening is detrainment from shallow to midlevel convection, the presence of which can be inferred from the erosion of the negative T_b anomaly around day −4. This type of behavior was noted by Raymond (1998) in a simple diabatic model of the tropical circulation. Before deep, precipitating convection could occur, the midtroposphere had to be moistened and saturated through a deep layer through the action of shallow convection. Convection in a dry environment tended to merely moisten the column rather than produce rain. Chen et al. (1996) saw a pattern of moistening similar to that of Fig. 6 during the three MJO events observed during the TOGA COARE IOP. The relative humidity between 950 and 700 mb increased slowly as the suppressed phase ended, and then the upper troposphere quickly moistened as deep convection began. Lin and Johnson (1996) reported the presence of shallow convective clouds before the onset of MJO convection in TOGA COARE. They found that, ''About 10 days after the suppressed period, convection gradually intensified . . . moistening occurred throughout most of the troposphere and warm anomalies can be observed in the middle and upper troposphere. Cool anomalies occurred near the surface and the tropopause.'' This is exactly the type of behavior seen here, both in water vapor and temperature, as will be discussed in the next section.

4) TEMPERATURE COMPOSITE

Figure 7 shows the composite temperature anomaly for the non-MC stations. During the suppressed period, there is a cold anomaly in the upper troposphere ex-

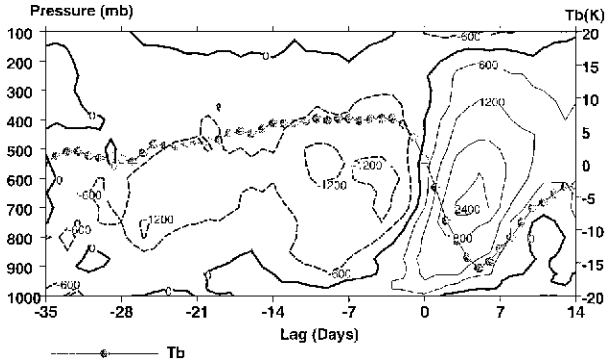

FIG. 8. Non–Maritime Continent station composite moist static energy and T_b anomalies. Thin solid contours indicate positive moist static energy anomaly and dashed contours indicate negative moist static energy anomaly. Thick solid line is the 0 contour. Contour interval is 600 J kg^{-1}.

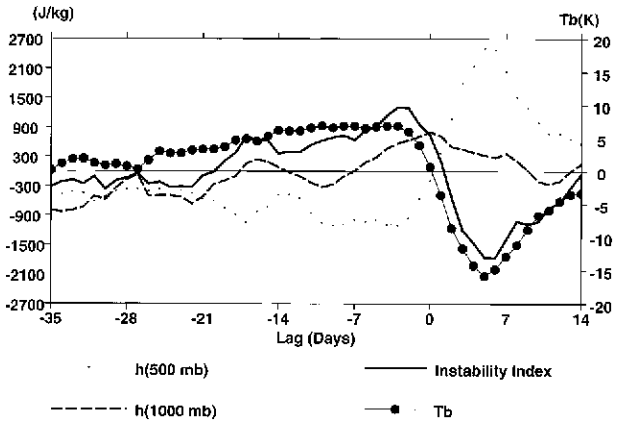

FIG. 9. Non–Maritime Continent station composite instability index, T_b anomaly, and moist static energy anomalies at 1000 and 500 mb.

tending from 200 mb down as low as 750 mb. This cold anomaly may be due to radiative cooling (Lin and Johnson 1996). Since the upper-level water vapor anomaly is negative during this time, cooling is consistent with a reduction in the trapping of longwave radiation.

The temperature anomaly signal in the surface–500-mb layer during the suppressed phase is not as coherent as that in the upper troposphere. Starting at about day -10, a weak warm anomaly develops in the lower troposphere and begins extending upward, reaching the 550-mb level by day 0. This coincides with the upward propagation of the positive specific humidity anomaly.

The convective phase of the MJO is marked by a layer of deep tropospheric warming extending from about 850 mb up to 200 mb, caused by latent heat release in deep convection. Beneath 850 mb, there is cooling that is likely due to the introduction of cold air by convective downdrafts (Betts 1976). Above 200 mb, there is cooling during the convective phase. Mapes and Houze (1992) found in a study of the Australian monsoon that the upper-tropospheric heating profile in mesoscale convective systems (MCSs) took the form of a ''cooling aloft during the convectively active periods. This may reflect a higher mean tropopause or possibly the mesoscale cold lens above individual tropical mesoscale convective systems.'' The CARDS station composite may be detecting the heating signature of the MCSs that are known to exist within the large-scale envelope of the convective phase of the MJO (Nakazawa 1988).

5) MOIST STATIC ENERGY COMPOSITE

The moist static energy (h) composite for the non-MC stations (Fig. 8) shows much the same behavior as the q composite (Fig. 6). This is because the moist static energy anomalies observed in this study were generally dominated by the term Lq, as composited temperature anomalies were less than 0.5 K in magnitude. A strong low h area extending up to about 300 mb appears around day -30 and is present until the onset of convection at day 0. One feature that shows up more clearly in the h plot than in the q plot is that, starting at day -20, a weak, positive h anomaly centered around 950 mb appears. It builds upward to about 850 mb by day -16 and is replaced around day -10 by a strong negative anomaly that lasts until a few days before the convection starts. A physical explanation for this feature is not readily apparent, but it appears in almost all of the individual station h composites, as well as being visible in the unfiltered station time series of h. The behavior of h after the onset of convection is similar to that of q, with a strong positive anomaly building upward in the troposphere. This maximum dies away by day $+20$.

6) STABILITY AND CONVECTION ONSET

b. Instability index composite

An instability index is formed by taking h(1000 mb) minus h(500 mb). This index is a simple measure of atmospheric instability analogous to the vertical gradient of the equivalent potential temperature, and its composite for non-MC stations is shown in Fig. 9. The convective available potential energy (CAPE) curve (not shown) closely follows the changes in the instability index. The CAPE tends to be noisier than the instability index, but their similarity suggests that the instability index is a reasonable gauge of atmospheric stability. The h index is more useful here in highlighting the relevant physics than is a bulk measurement of instability, such as CAPE, because the h index allows assessment of the importance of two specific layers of the atmosphere in determining the overall instability.

During the suppressed phase of the MJO, the instability index increases steadily (indicating that the atmosphere is becoming more unstable) until it reaches a maximum concurrent with the T_b anomaly. The insta-

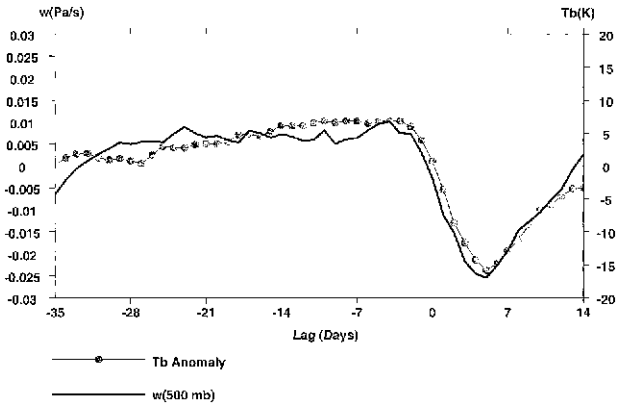

FIG. 10. Non–Maritime Continent station composite vertical velocity and T_b anomalies.

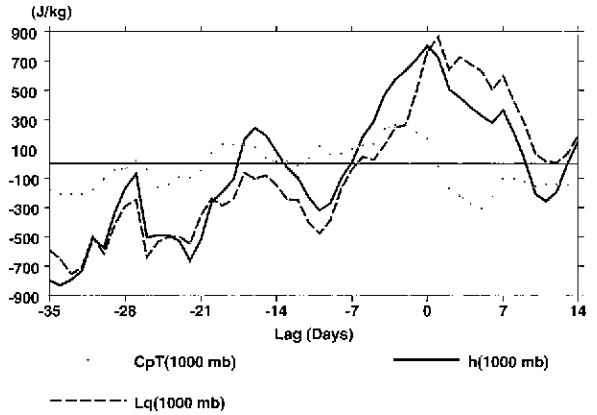

FIG. 11. Non–Maritime Continent station composite h(1000 mb), Lq(1000 mb), and C_pT(1000 mb) anomalies.

bility index roughly parallels the h(1000 mb) anomaly curve until day 0. Before the MJO convection begins, the h(1000 mb) curve shows a steady increase from negative to positive values, while the h(500 mb) remains negative until the onset of convection. As the MJO event begins, the h(500 mb) curve increases sharply, becoming positive and dominating the instability index.

The behavior of h(500 mb) can be partially interpreted by looking at the 500-mb vertical pressure velocity (ω) composite. Figure 10 shows anomalous upward motion during the convective event and anomalous sinking motion in the middle troposphere during the suppressed period. Spatial composites of ω(500 mb) and OLR (not shown) constructed using NCEP–NCAR reanalysis data suggest that this downward motion during the suppressed phase is due to subsidence caused by convection from the previous MJO cycle. NVAP precipitable water composites (not shown) do not show evidence for the advection of dry subtropical air by Rossby gyres spun up by the MJO convection as observed by Maloney and Hartmann (1998) or tongues of dry air intruding from the subtropics (Yoneyama and Fujitani 1995; Mapes and Zuidema 1996). This may be a result of the compositing procedure used here, which tends to average over smaller scale features. The anomalously low midtropospheric h during the suppressed phase of the MJO, then, may be caused by drying through subsidence. Once the subsidence is replaced by upward motion due to deep convection at day 0, the midtropospheric dry region is replaced by a region of positive moisture anomaly. While the h(1000 mb) undergoes a steady increase during the suppressed phase and peaks before convection starts, the h(500 mb) is unchanged until after the onset of convection. This result suggests that it is the buildup of low-level h, which controls the timing of the MJO convection. The free troposphere is anomalously dry during the suppressed phase due to large-scale sinking motion associated with the previous cycle of convection, and it is the combination of low upper-tropospheric h and the buildup of boundary layer h that creates the instability necessary for deep MJO convection.

All CARDS stations examined showed a substantial buildup in both 1000-mb moist static energy and instability throughout the suppressed period, with both reaching a peak within 3 days of day 0. This suggests that the increase in low-level moist static energy plays a critical role in the triggering of MJO convection. A key issue is the cause of the h(1000 mb) buildup. Figure 11 shows the non-MC station composite anomalies for T_b and 1000 mb C_pT and Lq (i.e., temperature and specific humidity scaled to be in units of J kg^{-1}), and moist static energy. Though there is considerable noise in the curves, all show a definite progression from negative anomalies to positive anomalies during the suppressed period, with the positive anomalies reaching a maximum or remaining near maximum as convection begins. All three 1000-mb anomalies drop off rapidly after day 0. Plots similar to Fig. 11 constructed for individual stations clearly show that the h anomaly is controlled by the Lq term, and that the buildup in h(1000 mb) and therefore instability, is caused by the buildup in q(1000 mb). The question then becomes, what is driving the increase in q(1000 mb) during the suppressed period? Two possible mechanisms for increasing q(1000 mb) are low-level convergence and surface fluxes. Convergence is addressed first, then surface fluxes.

c. Convergence

Based on the frictional wave–CISK theories of Wang and Li (1994) and Salby et al. (1994) and the observations of Maloney and Hartmann (1998), convergence at 1000 mb leads MJO convection near the equator. This phase shift is crucial to the generation of a positive low-level moisture anomaly that generates instability and predisposes the atmosphere to convection. Since the amplitude of frictional convergence at a particular station is a function of its distance from the equator, it is not reasonable to average over the stations to form a grand

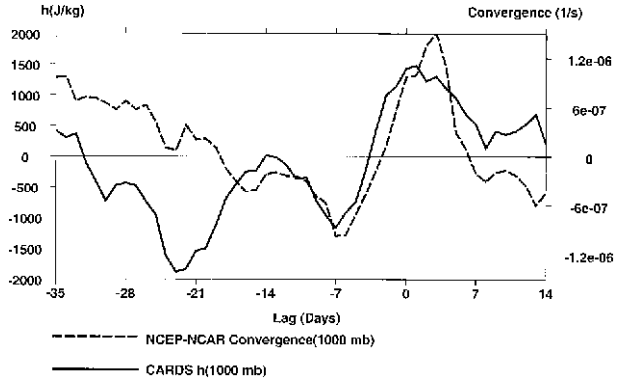

FIG. 12. Diego Garcia composite h(1000 mb) and NCEP–NCAR reanalysis convergence(1000 mb) anomalies. Positive anomalies correspond to convergence, negative anomalies to divergence.

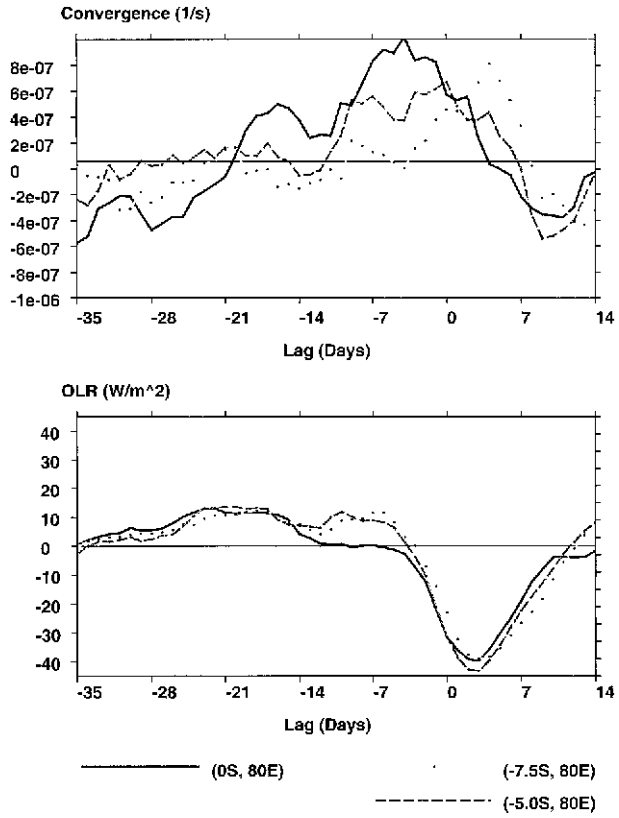

FIG. 13. NCEP–NCAR reanalysis 1000-mb convergence (top) and OLR (bottom) anomalies at 80°E.

mean of 1000-mb convergence. Therefore, we will investigate convergence composites for individual stations.

Figure 12 shows that, for Diego Garcia, the composited 1000-mb convergence does not lead the convection and reaches its maximum value within a day or two of the minimum in T_b. The peak in the convergence also lags the peak in the instability index, which coincides with the beginning of the erosion of the positive T_b anomaly at day -3. The timing of the maximum in the convergence suggests that convergence is not responsible for the steady increase in the 1000-mb moist static energy that occurs throughout the suppressed period. The convergence maximum seems to be a product of the convection, not its cause. This result holds true for all stations examined, including stations in the Indian Ocean, Maritime Continent, and the western Pacific. Based on individual station results similar to those shown in Fig. 12, it seems that different physical mechanisms may be responsible for increasing the low-level moist static energy off and on the equator.

To test the latitude dependence of this phase relationship between convection and low-level convergence, OLR and NCEP–NCAR 1000-mb convergence anomalies were examined for several locations in the Indian Ocean region where the original intensification of the convective anomaly usually occurs. Figure 13a shows the 1000-mb convergence anomaly for 80°E and 0°, −5.0°S, and −7.5°S. We chose 80°E because the MJO convective anomaly frequently intensifies near this longitude (Wang and Rui 1990). The OLR anomaly plots (Fig. 13b) for (0°, 80°E), (−5°S, 80°E), and (−7.5°S, 80°E) are similar in phase and intensity. The convergence peaks, however, are not in phase. The 1000-mb convergence anomaly peak at (0°, 80°E) leads the convergence anomaly peak at (−5°S, 80°E) by four days; the convergence anomaly peak at (0°, 80°E) leads the convergence anomaly peak at (−7.5°S, 80°E) by a full week. At (0°, 80°E), the 1000-mb convergence anomaly peak leads the OLR anomaly minimum by a week, while the 1000-mb convergence anomaly peak at (−7.5°S, 80°E) is in phase with the OLR anomaly minimum there. Plots similar to Fig. 13 were created for 70°E and 72.5°E, which are both in the Indian Ocean MJO amplification region. The results for these locations were similar to those for 80°E and are not shown. A plot similar to Fig. 13 for 90°E was similar to the (−7.5°S, 80°E) case. By the time the disturbance has reached 90°E it is no longer amplifying, and the convergence anomaly maxima are nearly in phase with one another and with the minima in the OLR anomaly.

The phase difference among the convergence anomaly maxima in Fig. 13a suggests that the physics of the MJO onset may be different for equatorial and off-equatorial locations. For the (0°, 80°E) case, it seems likely that frictional convergence is responsible for increasing the low-level moisture, contributing to instability that leads to MJO convection as shown by Maloney and Hartmann (1998). At (−7.5°S, 80°E), however, the phase relationship between the convergence and OLR anomalies suggest that convergence is not responsible for the generation of instability there. The progressive shift forward in time of the convergence peak as we move southward off the equator is consistent with the idea that frictional convergence becomes less important in creating instability as we move off the equator. Note

that the region of strong MJO convective variability encompasses off-equatorial as well as equatorial regions in the Tropics (Salby and Hendon 1994). A likely candidate for increasing q(1000 mb) during the suppressed phase of the MJO away from the equator is the flux of moisture from the warm tropical oceans into the atmosphere.

d. Surface fluxes

Observations show that a period of only 12–24 h is required for the boundary layer θ_e to recover from an episode of deep convection (Parsons 1994; Raymond 1995). If surface fluxes act to recharge the boundary layer moist static energy over a period of a day or less, why does the q(1000 mb) anomaly require 35 days to reach the point where convection is possible once more?

During the suppressed period, the composite h(1000 mb) is anomalously low, even though the previous convective event has long since passed (Fig. 9). Winds are light during the suppressed period and anomalous surface fluxes of heat and moisture are low (Zhang 1996). Meanwhile, there is anomalous large-scale subsidence aloft and anomalously dry air in a deep layer of the troposphere. It is possible that there are competing processes at work; surface fluxes act to slowly moisten the boundary layer, even as entrainment of dry air aloft tends to dry it out, the net result being a gradual increase of q(1000 mb) during the suppressed period. Raymond (1997) suggests that suppression of convection by subsidence over the tropical oceans is not due to the destruction of CAPE by subsidence, but instead to the suppression of boundary layer θ_e by entrainment of dry air aloft into the boundary layer.

5. Discussion

The radiosonde composites derived in this study suggest that the periodicity of the MJO may be partially controlled by the buildup and discharge of the low-level moist static energy, as hypothesized by Bladé and Hartmann (1993). Initiation of MJO convection at a station was most likely to occur when the atmosphere had been destabilized through a combination of low-level moist static energy buildup and simultaneous depression of the midtropospheric moist static energy.

Figure 14 is a schematic of the onset of MJO convection at an off-equatorial radiosonde station and is a summary of the results of this study. From day −35 to day −5, there is strong large-scale anomalous downward motion in the middle troposphere caused by subsidence from the previous cycle of MJO convection. This sinking motion creates a deep layer of anomalously low moist static energy.

Low-level easterly wind anomalies are present during the suppressed period from day −20 to day 0. Though light, these winds help to slowly moisten the boundary layer through the action of surface fluxes. We hypothesize that this moistening of the boundary layer is partially counteracted by entrainment of the anomalously dry air in the free troposphere into the boundary layer, and that the competition between the moistening and drying processes is responsible for the long recharge time of the boundary layer moisture and moist static energy (Fig. 11).

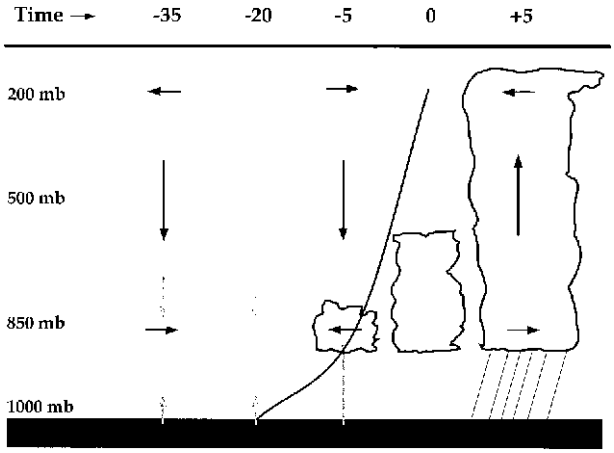

FIG. 14. MJO convection onset schematic. Dark horizontal arrows represent the zonal wind anomaly. Black vertical arrows are the 500-mb vertical velocity (omega) anomaly field. Solid gray vertical arrows represent the moistening of the boundary layer by surface fluxes, and dashed gray vertical arrows represent drying of the boundary layer by entrainment of overlying dry air. The curved black line is the dividing line between positive and negative moist static energy anomalies, with positive anomalies to the right of the line and negative anomalies to the left. The clouds represent shallow and deep, precipitating convection anomalies.

From day −35 to day −20, the moist static energy of the boundary layer is suppressed. By day −20, a positive moist static energy anomaly appears at 1000 mb, and by day −5, this 1000-mb moist static energy anomaly has grown large enough to generate shallow convection. Shallow convection transfers moisture upward out of the boundary layer, moistening the free troposphere and increasing its moist static energy. This preconditioning process is indicated in Fig. 14 by the upward slope of the solid, curved line.

By day +5, the next cycle of deep MJO convection is well under way. A strong, positive moisture anomaly moves well up into the troposphere. The 200-mb wind anomaly switches from westerly to easterly as the convection moves overhead, reflecting the outflow from the cumulus towers. There is strong anomalous low-level convergence collocated with the convection at day 0, and the anomalous 850-mb wind switches from easterly to westerly.

The station composites suggest that, for off-equatorial regions, the periodicity of MJO events may be at least partially set by the time it takes for the convective event to run its course added to the time needed for the h(1000 mb) to recharge and make the atmosphere unstable again. The recharge time for h(1000 mb) is largely con-

trolled by the recharge time for q(1000 mb), whose time constant may be the result of the competing processes of surface fluxes and entrainment of dry air into the boundary layer. Along the equator, we see the shift of 1000-mb convergence ahead of the convection predicted in frictional wave–CISK. Off the equator, however, this phase shift does not exist (Fig. 13), indicating that another mechanism, such as surface fluxes, may be responsible for initiating instability leading to convection there.

This study suggests that before a full MJO event can be initiated, off-equatorial regions must be ready to convect. This hypothesis is supported by the fact that there are many times during the 1975–90 time series of the NCEP–NCAR reanalysis 1000-mb convergence where a strong positive convergence anomaly was present along the equator, but no MJO event developed. Possibly, full MJO events may occur only when the off-equatorial atmosphere has been destabilized through the buildup of h(1000 mb) and the concurrent drying of the middle troposphere by subsidence from the previous MJO event. The combination of these two processes could produce an atmosphere that is ready to convect given a trigger, which may well be related to the convergence on the equator and the convection it produces. Given the tendency of convection to foster further convection (Randall and Huffman 1980; Mapes and Houze 1992; Mapes 1993), if equatorial convection exists at a time when the regions to the north and south are highly unstable, it is easy to see how a full-blown MJO event might develop. It may be that the energy source for the MJO is the eddy available potential energy (EAPE) generated by the equatorial disturbance (Salby et al. 1994; Hendon and Salby 1994), but that the period is set by the amount of time it takes the off-equatorial regions to regain their h(1000 mb) supply.

A key question is whether the convergence is in phase with the instability index along the equator when the disturbance is amplifying. Frictional wave–CISK theories predict that 1000-mb convergence should occur to the east of the convection. Then along the equator the 1000-mb convergence peak should lead the peak in the instability index in time. This is in contrast to the behavior shown in Figs. 9 and 12 for Diego Garcia, where the instability index peak leads that of the 1000-mb convergence.

Sufficient CARDS station data to form composites for equatorial stations was unavailable for the period 1988–90, so the NCEP–NCAR reanalysis dataset was used to calculate the h(1000 mb) anomaly there. However, when NCEP–NCAR data was compared against the CARDS station data for latitude–longitude pairs where a CARDS station exists, the phasing of the h(1000 mb) anomaly was found to be quite different (Fig. 15). The phase of h(1000 mb) was similar to that in Fig. 15 for all locations examined. In particular, the relationship between CARDS h(1000 mb) and the OLR does not change with latitude. These results suggest that

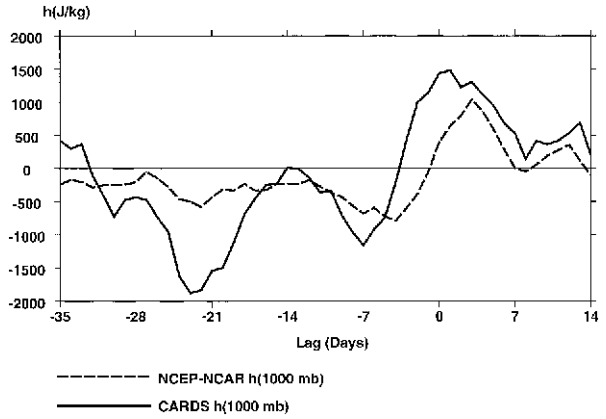

FIG. 15. Comparison of CARDS and NCEP–NCAR reanalysis h(1000 mb) anomalies.

the h(1000 mb) from the NCEP–NCAR reanalysis may be influenced more by model physics than station data, which are generally regarded as ground truth. The NCEP–NCAR data then may not be useful in assessing whether there is a buildup in h(1000 mb) along the equator before MJO events and, if so, whether it is caused by frictional moisture convergence.

This study suggests that local column effects may play a major role in the onset of the MJO off the equator, and this has ramifications for assessment of the aptitude of the various MJO theories. In particular, the lack of Kelvin wave signal at 200 mb preceding the convection weighs against wave–CISK theories that require a circumnavigating circulation anomaly to excite the next cycle of MJO convection. In their modeling study of frictional wave–CISK, Salby et al. (1994) suggest that an upper-level Kelvin signal is always present in the Tropics and ''amplifies through interaction with the climatological broadband heating when conditions become favorable over the Indian Ocean and the western Pacific.'' While no upper-level Kelvin signal was detected here, the MJO period does seem to be determined by the timing of the development of ''favorable conditions,'' which are deep instabilities caused by replenishment of moisture at low levels combined with cooling and drying in the middle and upper troposphere.

Maloney and Hartmann (1998) hypothesized that the timescale for the movement of the MJO convective anomaly from the Indian Ocean to the western Pacific may be set by the time required for frictional surface convergence to moisten the atmosphere in the western Pacific. This moistening preconditions the atmosphere for deep convection. The present study confirms that the moistening of the atmosphere seems to set the timescale, but for the CARDS stations we examined, low-level convergence does not cause the moistening. This may, of course, be due to the fact that all the stations in this study are located off the equator, where the effects of frictional convergence are less pronounced.

Neither frictional wave–CISK nor discharge–re-

charge mechanisms are ruled out by this study. In fact, both may play a role. The results here suggest that the discharge and recharge of moist static energy may be at least partially responsible for setting the period, while the energetics of the oscillation are controlled by equatorial frictional wave–CISK processes. Integrating these two types of theories may allow a more complete view of the physics of the MJO.

The other main result of this study is that there is evidence of transport of water vapor upward out of the boundary into the free troposphere preconditioning the atmosphere for deep convection as in TOGA COARE (Lin and Johnson 1996; Chen et al. 1996). This may have ramifications for parameterization of convection in GCMs, suggesting the importance of simulating shallow convective processes well. The shallow convection has a nonnegligible heating and moistening effect, which could have implications for the growth of waves simulated by GCMs (Brown 1994).

A worthwhile extension of this study would be to use sounding data from stations near the equator in the Indian Ocean and western Pacific, and construct composites similar to those in the present work. There are several CARDS stations (Maldives, Christmas Island, etc.) that lie near the equator but did not have sufficient data coverage to form stable composites for the time period (1988–90) used in this study. In particular, the phase of the peak in the instability index relative to that of the 1000-mb convergence should be compared with those of off-equatorial stations, as mentioned in section 4. This would be a good test of frictional wave–CISK theory and was not possible at the time of this study due to the lack of availability of CARDS data along the equator in the Indian Ocean.

Acknowledgments. We thank two anonymous reviewers whose comments helped to significantly improve this paper. NCEP–NCAR reanalysis data were provided by the NOAA–CIRES Climate Diagnostics Center, Boulder, Colorado, from their Web site at http://www.cdc.noaa.gov. NVAP water vapor data were obtained from the NASA Langley Research Center EOSDIS Distributed Active Archive Center. This work was supported by NSF Grant ATM-9613779 and a Campus Laboratory Collaboration grant from the University of California Office of the President.

REFERENCES

Betts, A. K., 1976: The thermodynamic transformation of the tropical subcloud layer by precipitation and downdrafts. *J. Atmos. Sci.*, **33,** 1008–1020.

Bladé, I., and D. Hartmann, 1993: Tropical intraseasonal oscillations in a simple nonlinear model. *J. Atmos. Sci.*, **50,** 2922–2939.

Brown, R., 1994: A modeling and observational study of convective interaction with large-scale dynamics in the Tropics. Ph.D. thesis, University of Washington, 192 pp.

Chen, S., R. Houze, and B. Mapes, 1996: Multiscale variability of deep convection in relation to large-scale circulation in TOGA COARE. *J. Atmos. Sci.*, **53,** 1380–1409.

Eskridge, R. E., and Coauthors, 1995: A comprehensive aerological reference dataset. *Bull. Amer. Meteor. Soc.*, **76,** 1759–1775.

Gill, A., 1980: Some simple solutions for heat-induced tropical circulations. *Quart. J. Roy. Meteor. Soc.*, **106,** 447–462.

Hartmann, D., and J. Gross, 1988: Seasonal variability of the 40–50 day oscillation in wind and rainfall in the Tropics. *J. Atmos. Sci.*, **45,** 2680–2702.

Hendon, H., 1988: A simple model of the 40–50 day oscillation. *J. Atmos. Sci.*, **45,** 569–584.

——, and M. Salby, 1994: The life cycle of the Madden–Julian oscillation. *J. Atmos. Sci.*, **51,** 2225–2237.

——, and B. Liebmann, 1990: A composite study of onset of the Australian summer monsoon. *J. Atmos. Sci.*, **47,** 2227–2240.

Hsu, H., B. Hoskins, and F.-F. Jin, 1990: The 1985/86 intraseasonal oscillation and the role of the extratropics. *J. Atmos. Sci.*, **47,** 823–839.

Hu, Q., and D. Randall, 1994: Low frequency oscillations in radiative-convective systems. *J. Atmos. Sci.*, **51,** 1089–1099.

Kalnay, E., and Coauthors, 1996. The NCEP/NCAR 40-Year Reanalysis Project. *Bull. Amer. Meteor. Soc.*, **77,** 437–471.

Kemball-Cook, S., 1999: The onset of convection in the Madden–Julian oscillation. Ph.D. thesis, University of California, Davis, 109 pp.

Knutson, T., and K. Weickmann, 1987: 30–60 day atmospheric oscillations: Composite life cycles of convection and circulation anomalies. *Mon. Wea. Rev.*, **115,** 1407–1436.

——, ——, and T. Kutzbach, 1986: Global scale intraseasonal oscillations of outgoing longwave radiation and 250-mb zonal wind. *Mon. Wea. Rev.*, **114,** 605–623.

Liebmann, B., and C. Smith, 1996: Description of a complete (interpolated) OLR dataset. *Bull. Amer. Meteor. Soc.*, **77,** 1275–1277.

Lin, X., and R. Johnson, 1996: Heating, moistening, and rainfall over the western Pacific warm pool during TOGA COARE. *J. Atmos. Sci.*, **53,** 3367–3383.

Madden, R., and P. Julian, 1971: Detection of a 40–50 day oscillation of the zonal wind in the tropical Pacific. *J. Atmos. Sci.*, **28,** 702–708.

——, and P. Julian, 1972: Description of global-scale circulation cells in the tropics with 40–50 day period. *J. Atmos. Sci.*, **29,** 1109–1123.

——, and P. Julian, 1994: Observations of the 40–50-day tropical oscillation—A review. *Mon. Wea. Rev.*, **122,** 814–837.

Maloney, E., and D. Hartmann, 1998: Frictional moisture convergence in a composite life cycle of the Madden–Julian oscillation. *J. Climate*, **11,** 2387–2403.

Mapes, B., 1993: Gregarious tropical convection. *J. Atmos. Sci.*, **50,** 2026–2037.

——, and R. Houze, 1992: An integrated view of the 1987 Australian monsoon and its mesoscale convective systems. I: Horizontal structure. *Quart. J. Roy. Meteor. Soc.*, **118,** 927–963.

——, and P. Zuidema, 1996: Radiative-dynamical consequences of dry tongues in the tropical troposphere. *J. Atmos. Sci.*, **53,** 620–638.

Nakazawa, T., 1988: Tropical superclusters within intraseasonal variations over the western Pacific. *J. Meteor. Soc. Japan*, **66,** 823–839.

Nitta, T., T. Mizuno, and K. Takahashi, 1992: Multi-scaled convective systems and the 86/87 ENSO. *J. Meteor. Soc. Japan*, **70,** 447–458.

Parsons, D., and Coauthors, 1994: The Integrated Sounding System: Description and preliminary observations from TOGA COARE. *Bull. Amer. Meteor. Soc.*, **75,** 553–567.

Press, W., S. Teukolsky, W. Vetterling, and B. Flannery, 1986: *Numerical Recipes.* Cambridge Press, 963 pp.

Randall, D., and G. Huffman, 1980: A stochastic model of cumulus clumping. *J. Atmos. Sci.*, **37,** 2068–2078.

Raymond, D., 1995: Regulation of convection over the West Pacific warm pool. *J. Atmos. Sci.*, **52,** 3943–3959.

——, 1997: Boundary layer quasi-equilibrium. *The Physics and Pa-*

rameterization of Moist Atmospheric Convection, R. Smith, Ed., Kluwer Academic Publishers, 498 pp.

——, and D. Torres, 1998: Fundamental moist modes of the equatorial troposphere. *J. Atmos. Sci.,* **55,** 1771–1790.

Rossow, W., and L. Gardner, 1993: Cloud detection using satellite measurements of infrared and visible radiances from ISCCP. *J. Climate,* **6,** 2370–2393.

Rui, H., and B. Wang, 1990: Development characteristics and dynamic structure of tropical intraseasonal convection anomalies. *J. Atmos. Sci.,* **47,** 33–61.

Salby, M., and H. Hendon, 1994: Intraseasonal behavior of clouds, temperature, and motion in the Tropics. *J. Atmos. Sci.,* **51,** 2207–2224.

——, R. Garcia, and H. Hendon, 1994: Planetary-scale circulations in the presence of climatological and wave-induced heating. *J. Atmos. Sci.,* **51,** 2344–2367.

Waliser, D., K. Lau, and J. Kim, 1999: The influence of coupled sea surface temperatures on the Madden–Julian oscillation: A model perturbation experiment. *J. Atmos. Sci.,* **56,** 333–358.

Wang, B., and T. Li, 1994: Convective interaction with boundary layer dynamics in the development of a tropical intraseasonal system. *J. Atmos. Sci.,* **51,** 1386–1400.

——, and H. Rui, 1990: Synoptic climatology of transient tropical intraseasonal convective anomalies: 1975–1985. *Meteor. Atmos. Phys.,* **44,** 43–62.

Wang, W., and M. Schlesinger, 1999: The dependence on convection parameterization of the tropical intraseasonal oscillation simulated by the UIUC 11-layer atmospheric GCM. *J. Climate,* **12,** 1423–1457.

Yanai, M., S. Esbensen, and J.-H. Chu, 1973: Determination of bulk properties of tropical cloud clusters from large-scale heat and moisture budgets. *J. Atmos. Sci.,* **30,** 611–627.

Yoneyama, K., and T. Fujitani, 1995: The behavior of dry westerly air associated with convection observed during the TOGA COARE R/V *Natsushima* cruise. *J. Meteor. Soc. Japan,* **73,** 291–304.

Zhang, C., 1996: Atmospheric intraseasonal variability at the surface in the tropical western Pacific Ocean. *J. Atmos. Sci.,* **53,** 739–758.

——, and H. Hendon, 1997: Propagating and standing components of the intraseasonal oscillation in tropical convection. *J. Atmos. Sci.,* **54,** 741–752.